Acta of Bioengineering and Biomechanics
Vol. 24, No. 1, 2022

Original paper
DOI: 10.37190/ABB-01962-2021-03

Analysis of friction and wear processes in an innovative spine stabilization system. Part 1. A study of static and kinetic friction of a metal rod-polymer cord friction joint

ANNA BROŃCZYK*

Wrocław University of Science and Technology, Faculty of Mechanical Engineering, Wrocław, Poland.

Purpose: This analysis is the first part of research that aims to develop a model of the tribological wear of PE-UHMW cord – biometal rod combination. This type of sliding joint is applied in spine stabilization systems that enable the treatment of early-onset idiopathic scoliosis. *Methods*: The friction tests included force measurements, followed by the determination of static and kinetic friction coefficients as a function of the number of the performed movement cycles, and static friction coefficient with regards to the string tension force FN in the range of 50–300 N. Additionally, the surface roughness and microscopic observations of the metal rods were made. The friction measurements were carried out at a stabilized temperature T = 38 °C in the presence of distilled water and acidic sodium lactate. *Results*: The measurements confirmed the impact of both the number of completed movement cycles and the value of the force loaded on the cord on the static friction coefficient. Similar values of kinetic friction force occur for the pairs with the titanium alloys rods, as well as for the pairs with the steel and CoCr rod. The type of lubricant affected the obtained measurement results unevenly: (Ti6Al4V and Ti6Al7Nb – slight impact, steel 316L and CoCrMo – large impact). During microscopic observations, numerous wear products, were visible, including harder than the base material large conglomerates. *Conclusions*: Susceptibility of polymer fibres results in its increased resistance to wear, but it can be also combined with an increase in wear of the surface of the metal rod.

Key words: *friction, polymer fibres, 316L, Ti6Al4V, Ti6Al7Nb, CoCrMo*

1. Introduction

Despite the enormous recent progress made in medicine and biomedical engineering, the problem of treating early-onset idiopathic scoliosis has not been properly addressed. It is not easy to reconcile the need to stabilize the treated section with the need for mobility. Traditional stabilization systems, which can be successfully used in adult patients, cannot be applied in this case, because they contribute to blocking process of growth [9], [17], [21]. Its unblocking can be associated with the necessity to perform numerous reoperations and constant corrections of the already applied correction settings. If this was not done, not only would the already obtained correction be lost, but even new spine curvatures can be induced. In such cases, so-called guided-growth implants are used. Rohlmann et al. [21] described a stabilization system based on metal-metal friction joints, in which longitudinal rods and mobile connectors played the role of a slide bearing. In turn, Meijer [17], Bogie et. al [4], Roth et al. [22] focused on a stabilization system using polymer-metal friction joints. The assumption of such stabilization systems is to ensure correction and stabilization, while at the same time allowing for spinal elongation. This is usually achieved by completely blocking the rods that are fixed in the lowest position. At the same time, the remaining fastening elements, which are implanted into the vertebrae that are located

* Corresponding author: Anna Brończyk, Wrocław University of Science and Technology, Faculty of Mechanical Engineering, ul. Łukasiewicza 5/7, 50-370 Wrocław, Poland. E-mail: anna.bronczyk@pwr.edu.pl
Received: November 18th, 2021
Accepted for publication: February 10th, 2022

higher, are kind of guides that allow for the correct growth of the spine. An example of guided-growth stabilization is the solution proposed in the BMM SpineGuide® project (Fig. 1).

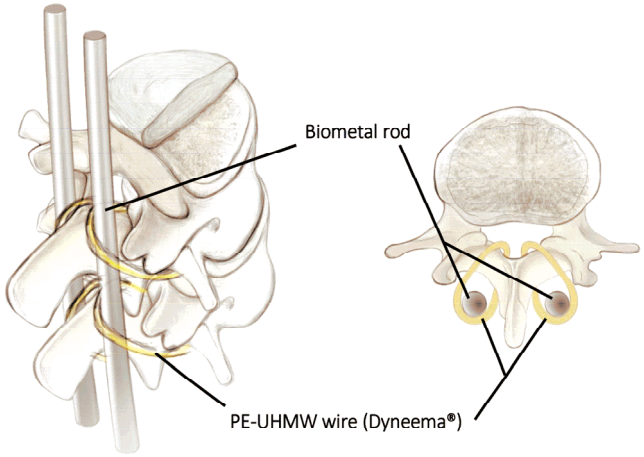

Fig. 1. The guided-growth stabilizer is fixed according to the SpineGuide® design

The polymer wire fixes the biometal rod to the vertebral curvature. The deformation is corrected by stretching the polymer cords. The cord can slide along the rod.

The operating principle consists in the sliding cooperation of the PE-UHMW cord with a biometal rod and was described in papers [4], [17], [23]. This solution is based on the frictional PE-UHMW–metal combination, which has already been tested for joint endoprostheses. In this solution, movable joints are metal rods, which are fixed to the spine with wires made of PE-UHMW fibres.

Non-fusion stabilization systems apply the relative movement of the components. As a result, tribological problems arise due to the friction that is generated between the components of the stabilizing system. Bogie et al. [3] described cases of serve metallosis, which occurred as a result of the use of guided-growth stabilizers, in which the sliding joints were elements made of an alloy of titanium and CoCr.

Current research on the tribological properties of implants is most often carried out in the following areas: the selection of materials for frictional pairs, and their evaluation in terms of tribological properties [12], [15], [16], [26] or the impact of frictional wear products on the peri-implant tissues [7], [19], [20], [25]. It should be stressed that these studies are conducted mainly in relation to joint endoprostheses.

Research on polymer fibres is usually conducted regarding physical, chemical and mechanical properties [7], [18], [29] as well as bio-acceptability [27]. Tribological properties, on the other hand, are mainly studied in relation to composites reinforced with polymer fibres [6], [8], [10], [11], [28].

The aim of the work is to determine the basic tribological properties of biometal rods and cords made of PE-UHMW fibres, which are used in spinal stabilization systems for the treatment of early-onset scoliosis.

This article focuses on the frictional resistance of guided-growth stabilization systems and is the first of two parts of research into the processes of the friction and wear of the sliding connection between a metal rod and polymer cord. Its scope includes measurements of static and kinetic friction forces, roughness measurements, and microscopic observations of the surface of the metal rod before and after the friction process.

2. Materials and methods

Friction joints, which are found in modern spine stabilization systems that use PE-UHMW cords to fix biometal rods, are an interesting case in terms of tribological properties. On the one hand, it is important to ensure proper correction and stabilization, i.e., to immobilise the section to be stabilized, but on the other hand, to allow for relative movement of adjacent surfaces so as not to block the process of spinal growth. Thus, in these types of solutions, alternating states of rest and movement occur, in turn causing the transformation from static friction to kinetic friction. Therefore, one of the most important parameters characterising these phenomena will be static and kinetic friction coefficients. Both friction coefficients were determined in an indirect way using friction forces.

Moreover, polymer fibres, while sliding on a metal rod, remain under constant tension, which can significantly affect their wear resistance [14].

In order to determine the frictional resistance in modern spine stabilization systems, using tribological joints of biometal solid material – polymer cord, the following tests were carried out:

- measurements of the static friction force,
- measurements of the kinetic friction force,
- determination of the change in roughness of biometal rods,
- microscopic observations of the rod surface before and after the friction process.

The rod material was selected from the three most popular biometal groups, i.e., austenitic steel 316L,

Table 1. Chemical compositions of the rods subjected to friction testing

Material Norm	Mass concentration [%]										
Ti6Al4V ISO 5832-3	Al 6.75	V 4.5	Fe 0.3	O 0.2	C 0.08	N 0.05	H 0.009	Ti remainder			
Ti6Al7Nb ISO5832-11	Al 6.5	Nb 7.5	Ta 0.5	Fe 0.25	O 0.2	C 0.08	N 0.05	H 0.009	Ti remainder		
CoCrMo ISO 5832-12	Cr 30	Mo 7	Fe 0.75	Mn 1	Si 1	C 0.14	Ni 1	N 0.25	Co remainder		
316L ISO 5832-1	C 0.03	Si 1	Mn 2	P 0.025	S 0.01	N 0.1	Cr 19	Mo 3	Ni 15	Cu 0.5	Re remainder

Table 2. Values of parameters at which the friction tests were carried out

	Kinetic		Static
F_N	300 N		50 N, 100 N, ..., 300 N
v_s	0.005 m/s		–
T	38 °C ± 2 °C		38 °C ± 2 °C
N° of cycles	1000 5000 10 000 20 000		–
Initial rod roughness			
Ti6Al4V	Ti6Al7Nb	316L	CoCrMo
Sq = 0.716 μm	Sq = 0.622 μm	Sq = 0.463 μm	Sq = 0.822 μm

two titanium alloys Ti6Al4V and Ti6Al7Nb, and cobalt alloy CoCrMo. In the course of the friction measurements, the rods slid against the cord made of PE-UHMW (Dyneema®) fibres. The chemical compositions of the alloys used for the rods are shown in Table 1.

The tested rods were supplied by a company that produces implants and tools used in orthopaedics (ChM®, Juchnowiec Koscielny, Poland).

In order to recreate the conditions in the human body, two types of solutions were used – distilled water and acidic sodium lactate. Their task was to simulate the normal state (distilled water) and inflammation (acidic sodium lactate) in the body. Distilled water is the substance commonly used for tests to simulate the effects of body fluids. Moreover, due to the fact that the results obtained with its use are characterized by considerable stability, it is recommended by the authors of paper [20] as the substance most suitable for determining tribological characteristics. Additionally, the ASTM F1089–10 norm indicates it as a factor suitable for corrosion testing of surgical instruments.

Acidic sodium lactate (ASL), on the other hand, is an organic compound commonly used in the cosmetics (as a moistening agent) and food industries (preservative E325). It consists of lactic acid (1/10 M) and sodium chloride (1/10 M). In research on corrosion and tribocorrosion, it serves as a medium that simulates the environment in which organic substances are found, while in biological research, thanks to its acidic pH (approx. 2), it can reproduce the situation of inflammation [5], [24], [30]–[32].

The surfaces of the rods were degreased with ethyl alcohol before testing.

Tribological tests of the friction pairs under examination were carried out using the parameter values presented in Table 2.

The values of the forces applied in the experiment were accepted on the basis of the Stotte's load model estimation [1] and calculations included in publication [2] for an individual weighing 76 kg. These loads were imposed by the head, shoulders and torso during a forward bend at the level of the L5 vertebrae. The obtained force value, at the level of about 2000 N, concerns the stabilization system proposed in the BMM SpineGuide® project, in which a metal rod is fixed to the spine with PE-UHMW cords. In the experiment carried out for the purpose of this work, these loads were assumed to be the total of all the fixing cords. It was assumed that force F_N exerted on one cord was up to 300 N. This corresponds to the use of a minimum of seven loops in the spine stabilization system.

The maximum number of 20,000 operating cycles for one year of use was assumed with an average of 55 operating cycles per day (bend and return), which cause the cord to move along the rod in the tested stabilization system.

The testing plan is shown in Fig. 2.

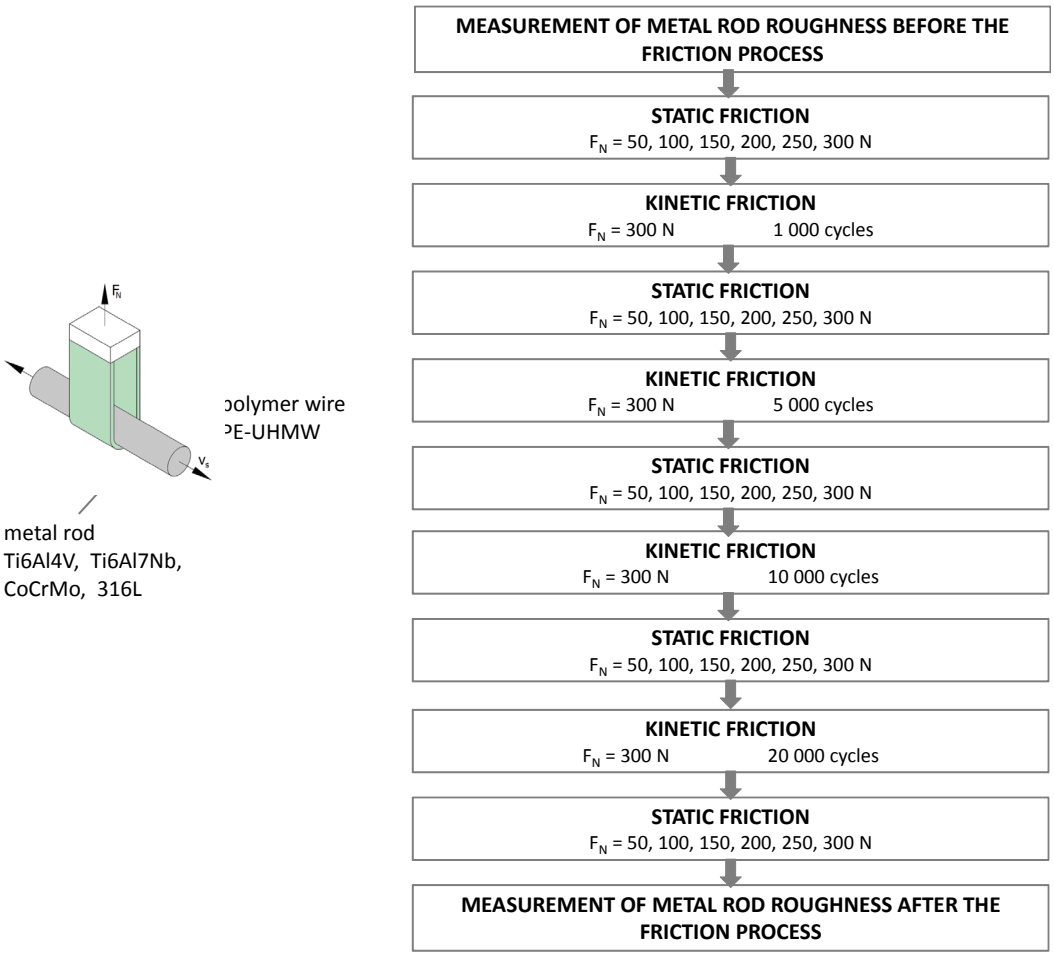

Fig. 2. Testing plan for the friction and wear of the tribological joints of the solid material and PE-UHMW wire

2.1. Friction testing

The friction measurements included measurements of the static F_{F0} and kinetic F_F friction forces. These values were then used to determine the static μ_0 and kinetic μ friction coefficients. For this purpose, an innovative device for testing the friction of fibres and braided wires was constructed (Fig. 3), submitted to the Polish Patent Office under the number P415423, and described in more detail in publication [13], which made it possible to simulate the wire's movement along the rod.

The arithmetic mean of about 30 maximum friction forces occurring in the sliding and rolling movement, during gradual increase of the axial force acting

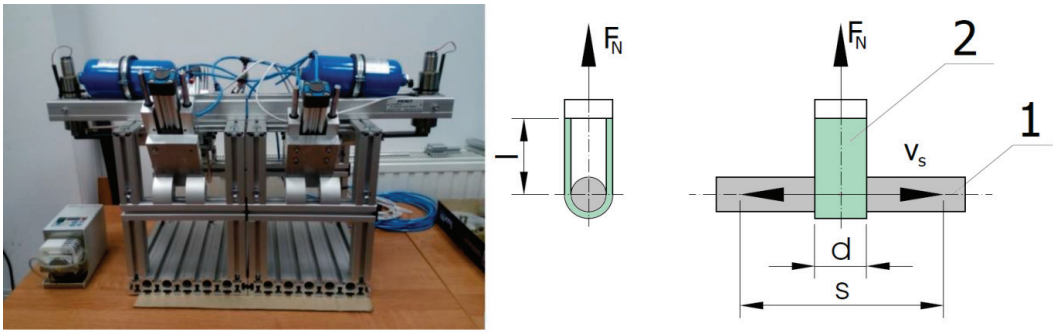

Fig. 3. On the left: friction testing stand for fibres and braided wires; On the right: diagram of the tribological node used: 1 – tested rod, 2 – polymer wire, b – wire width, d – wire diameter, l – wire length from the handle, s – length of movement cycle, F_N – wire tension force, F_F – friction force, v_s – average sliding speed

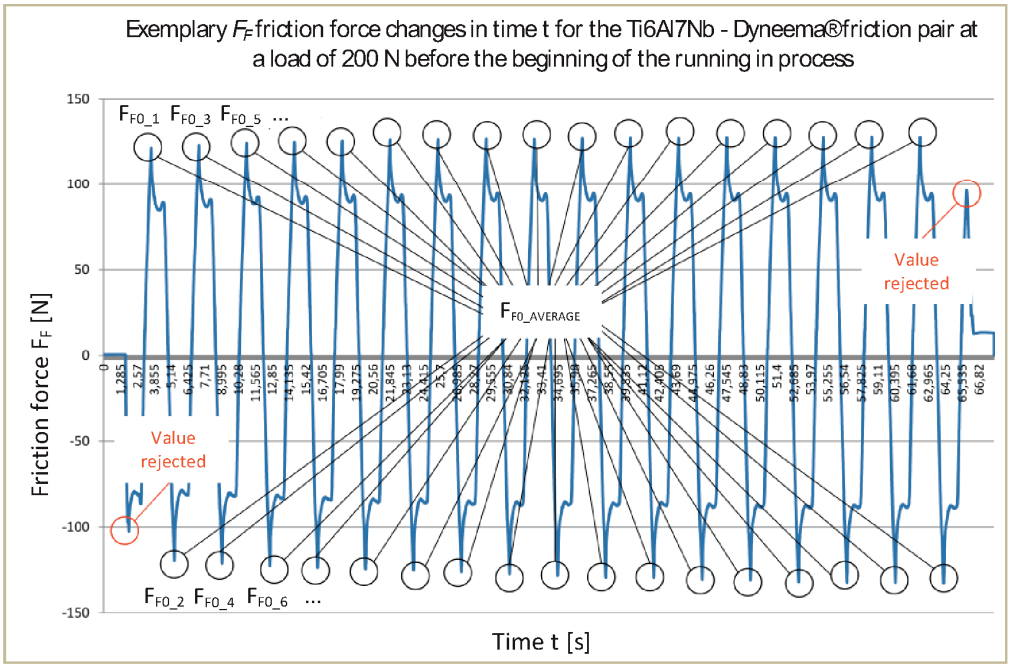

Fig. 4. Method of determining the static friction force

on the rod until a relative displacement between the wire and the rod appears, was taken as the static friction force value. The first and last maximum value was discarded according to the procedure adopted in the measurements. This procedure is illustrated in Fig. 4.

The kinetic friction force was determined as a median of the values recorded during the measurements. An example of its course is shown in Fig. 5 using a moving average.

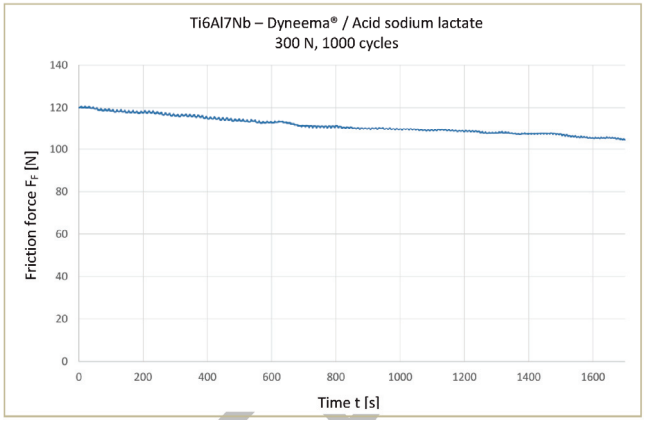

Fig. 5. Example of the kinetic friction force change for the sliding pairs: Ti6Al7Nb rod – Dyneema® wire in an acidic sodium lactate environment, under a load of F_N 300 N during 1000 movement cycles

The static friction coefficient μ_0 was determined as the quotient of the static friction force F_{F0} and the wire tension force F_N, and the kinetic friction coefficient μ was determined as the quotient of the kinetic friction force F_F and the wire tension force F_N, according to formula (1):

$$\mu = \frac{F_F}{F_N}. \tag{1}$$

2.2. Roughness measurements

In order to supplement the information on the sliding cooperation of the tested combinations, the surface roughness of the biometal rods was measured before and after the friction process. In order to determine the change in the roughness of the rod surface, an area of approximately 800 × 600 μm was scanned with the Leica DCM8 optical profilometer (Leica Camera AG, Wetzlar, Germany). To this end a confocal system with a 20 times magnification lens was used. The data obtained by scanning was then processed. For this purpose, the Leica MAP DCM software was applied, with the levelling and shape removal functions, to eliminate the influence of the cylindrical geometry of the rod on the roughness parameters values. The final stage of roughness measurements was the generation of a contour and topographic map of the studied area and the determination of linear and surface roughness parameters (*Ra*, *Sa* and *Sq*). The linear roughness parameter, *Ra*, was determined based on three roughness profiles measured in the direction of friction (i.e.,

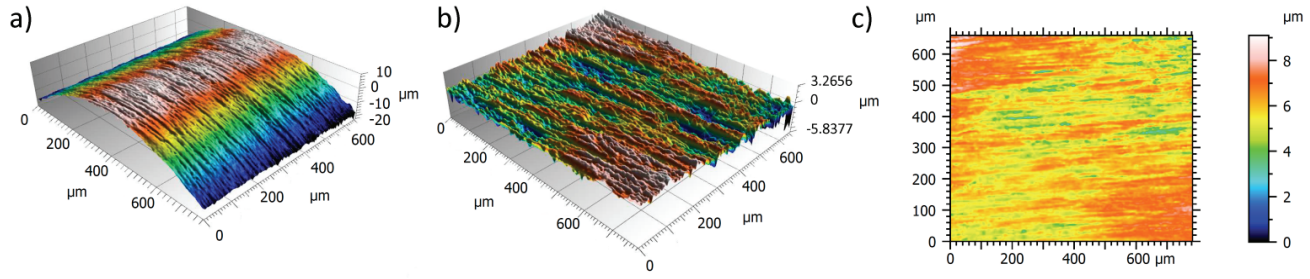

Fig. 6. Surface roughness for CoCrMo rod before friction process: a) measured surface of the rod, b) surface axonometric view after removing/filtering out the cylindrical form, c) surface map

along the rod). Roughness measurements were made before and after the friction process was completed. Process of measuring the surface roughness for the CoCrMo rod before the friction process is illustrated in Fig. 6.

2.3. Microscopic observation of the metal rod surface

Microscopic observations of the rod surface were carried out using a scanning electron microscope (Phenom ProX, Phenom-World B.V., Eindhoven, the Netherlands). They were performed before the friction process and after 20,000 movement cycles, which corresponds to the long-term lifetime of an implant. The tests were carried out in the low vacuum mode (LV-SEM) on non-sputtered rods.

3. Results

3.1. Measurement of static friction

The results of the static friction measurements are presented in Fig. 7. The presented graphs show the correlation of the static friction coefficient on the wire tension force for different friction pairs and lubricating agents, and also on the number of movement cycles completed.

3.2. Kinetic friction tests

The results of measurements of kinetic friction in the environment of acidic sodium lactate and distilled water are presented collectively in Fig. 8 for all the tested friction pairs. The graphs show the correlation between the kinetic friction coefficient and the number of movement cycles performed, while also comparing the friction pairs with each other.

The diagrams presented in Fig. 9 show a comparison of the values of the kinetic friction coefficients for a given sliding combination with regards to the used solution.

3.3. Measurement of the surface roughness of metal parts

In order to analyze changes on the rod surface, after filtering the bar curvature, selected roughness parameters were determined. The values of the *Ra*, *Sq* and *Sa* parameters measured before and after the friction process are presented in Table 3. The value of the *Ra* parameter was determined as the arithmetic mean of the three profiles and compiled together with the standard deviation value.

Table 3. Roughness values of selected biometal rods

		Roughness parameters [µm]		
		Initial	Acidic sodium lactate	Distilled water
316L	*Ra*	0.09 ± 0.024	0.078 ± 0.01	0.191 ± 0.096
	Sq	0.463	0.432	0.841
	Sa	0.355	0.319	0.602
CoCrMo	*Ra*	0.333 ± 0.111	0.158 ± 0.009	0.205 ± 0.109
	Sq	0.822	0.545	0.712
	Sa	0.653	0.404	0.535
Ti6Al4V	*Ra*	0.256 ± 0.051	0.29 ± 0.024	0.248 ± 0.085
	Sq	0.599	0.892	0.632
	Sa	0.459	0.695	0.481
Ti6Al7Nb	*Ra*	0.286 ± 0.026	0.371 ± 0.003	0.357 ± 0.052
	Sq	0.662	0.897	0.684
	Sa	0.504	0.683	0.527

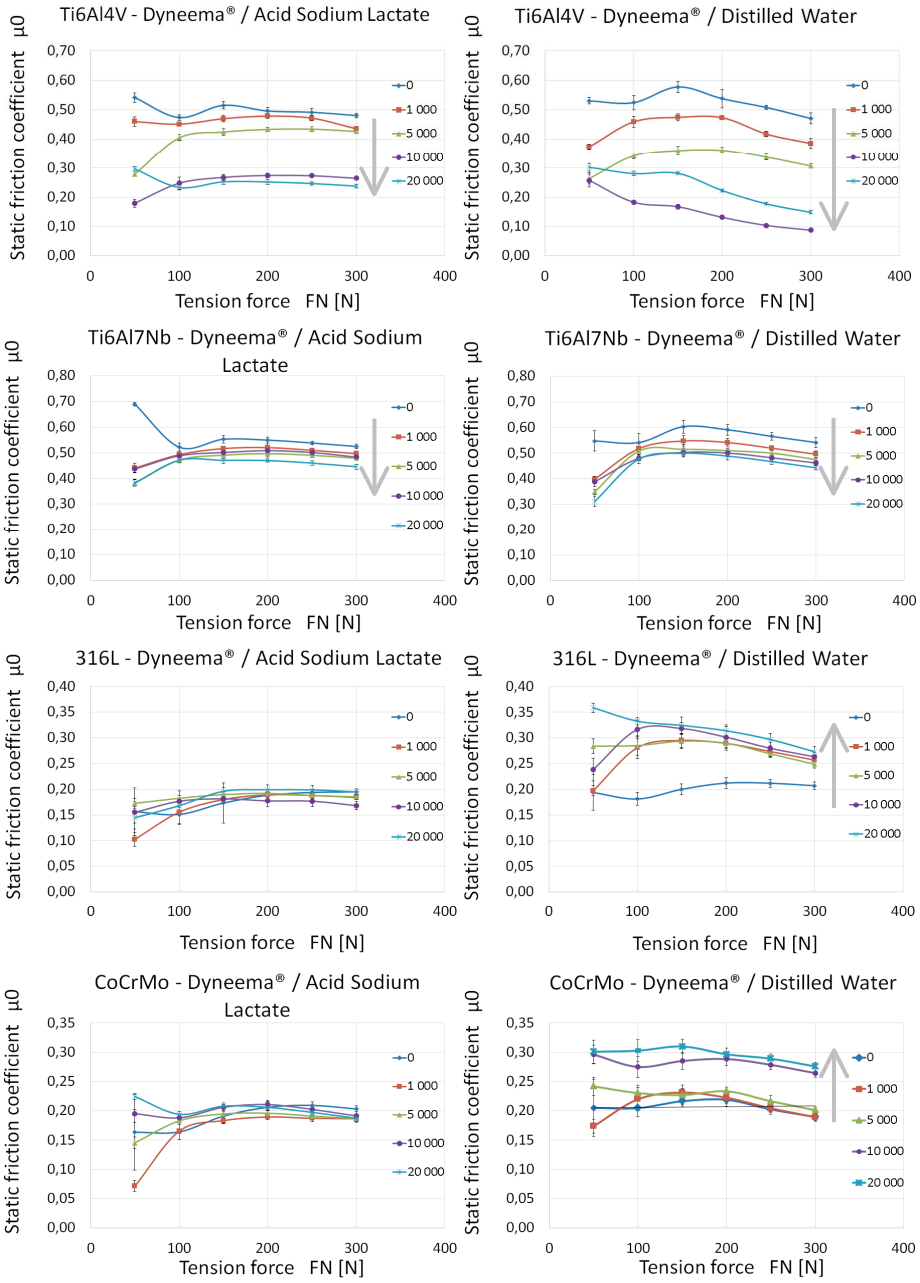

Fig. 7. Impact of tension force on the static friction coefficient for the tested sliding pairs in the presence of acidic sodium lactate (left) and distilled water (right)

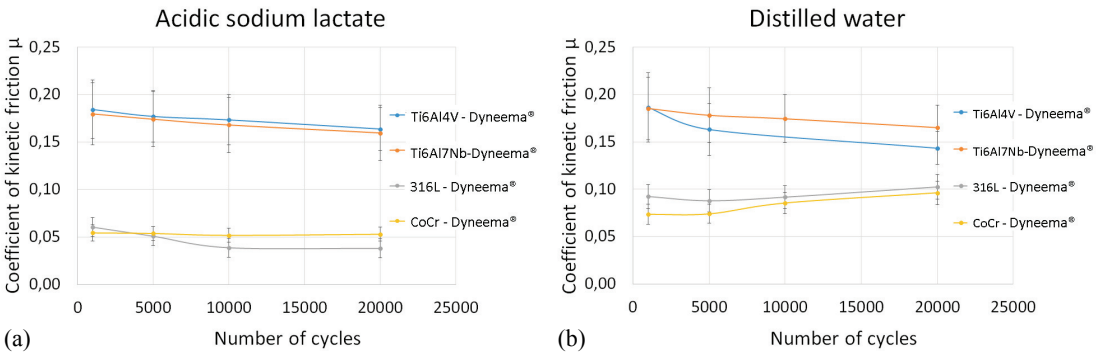

Fig. 8. Impact of the number of completed movement cycles on the value of the kinetic friction coefficient with regards to the type of frictional combination in the environment: (a) acidic sodium lactate, (b) distilled water

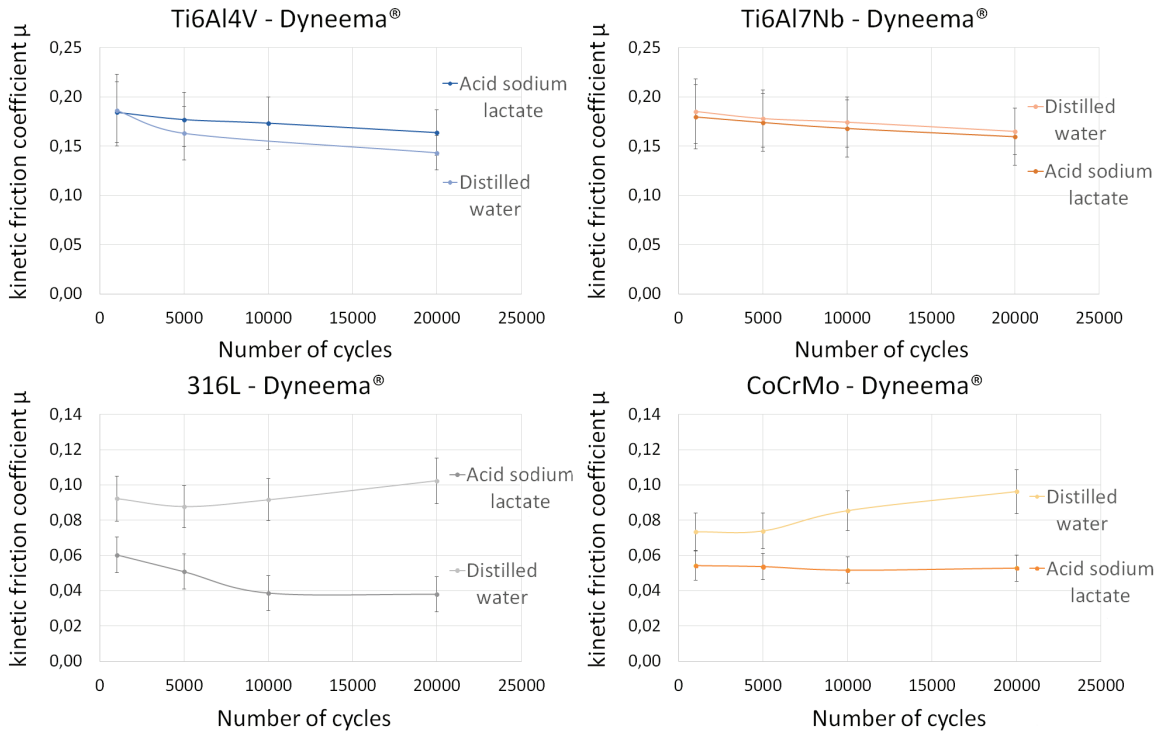

Fig. 9. Comparison of the values of the kinetic friction coefficients of the tribological node: metal rod – Dyneema® polymer wire for different solutions

3.4. Microscopic observations of the rod surface

The results of microscopic observations are shown in Figs. 10–18. The images show the changes that occurred on the surface of the metal rod due to its frictional interaction with the PE-UHMW wire. The pictures were taken at various magnifications.

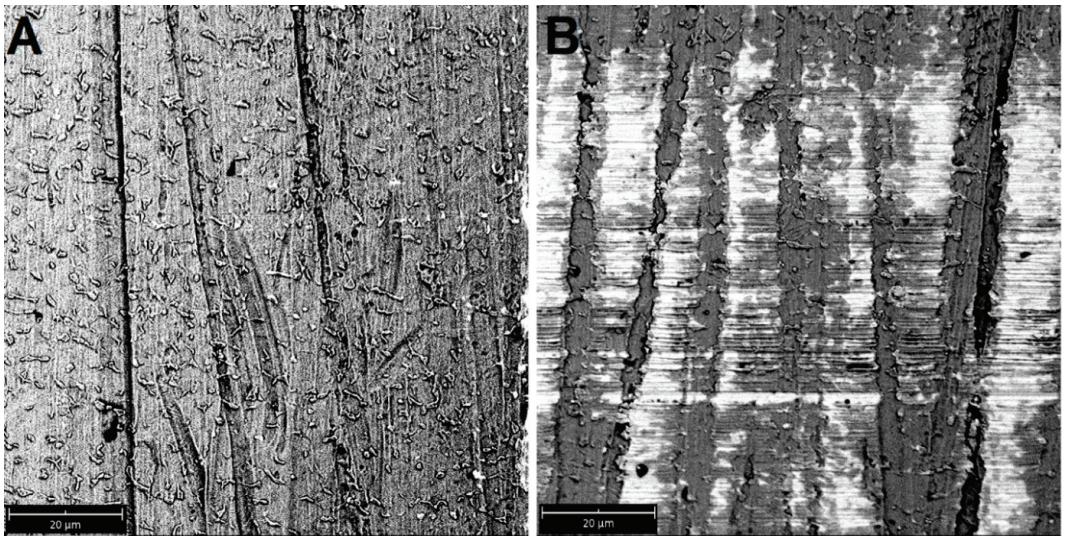

Fig. 10. Surface of the Ti6Al4V alloy rod: A – before the friction process, B – after friction in an environment of acidic sodium lactate; uneven distribution of pressures in the friction area is visible

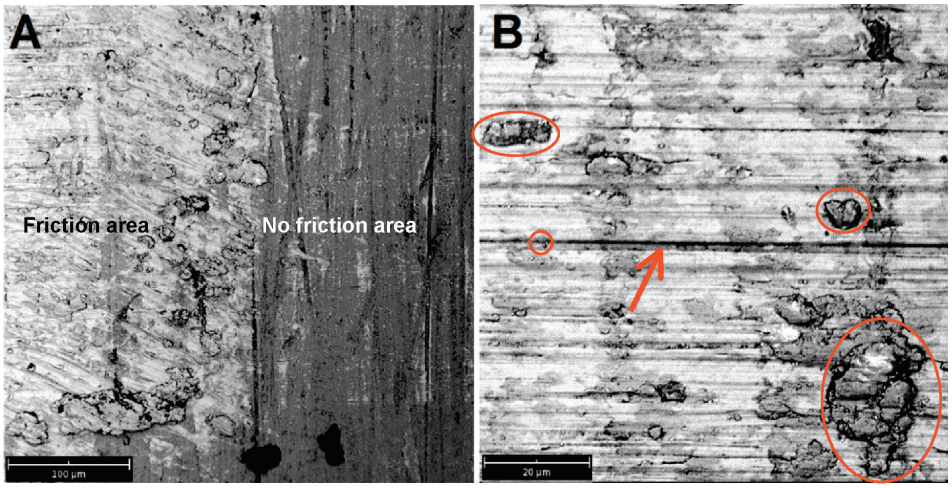

Fig. 11. Surface of the Ti6Al4V alloy rod: A – visible border between the friction and non-friction areas, B – surface damage caused by the friction process; red oval marks indicate single wear products and conglomerated ones, and the arrow shows the effect of furrowing; friction in distilled water

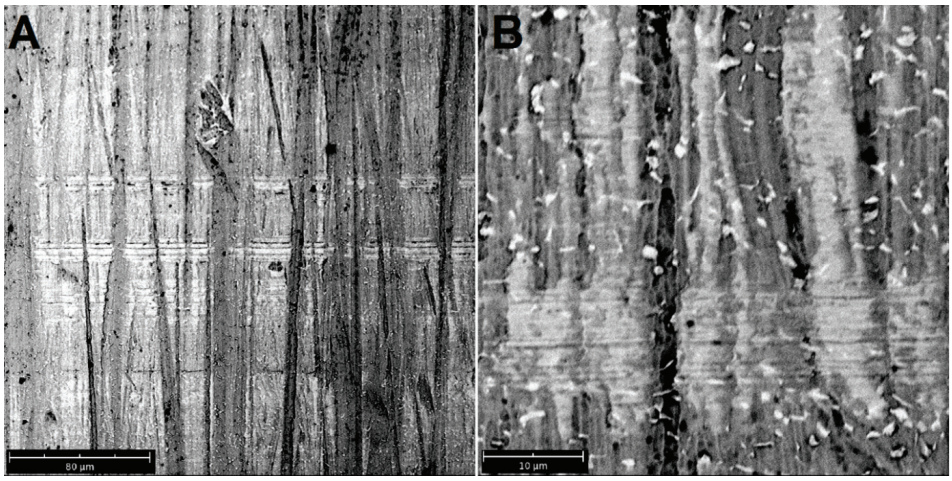

Fig. 12. Surface of the Ti6Al7Nb alloy rod: A – visible uneven distribution of pressures in the friction area, B – smoothing of the surface caused by flattening the tops of the uneven structure; friction in the presence of acidic sodium lactate

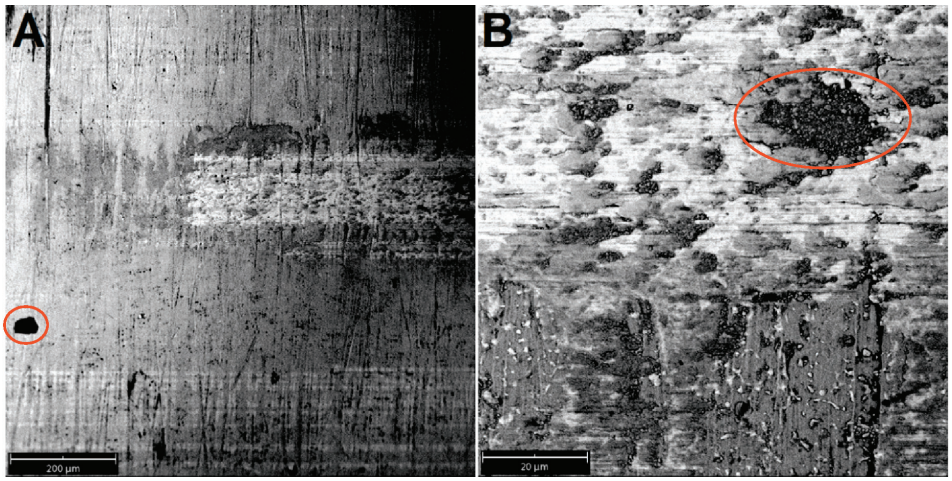

Fig. 13. Surface of the Ti6Al7Nb alloy rod: A – visible uneven distribution of pressure in the friction area; unevenness visible both along and across the direction of movement; red colour marks the wear product with a significant size of about 80 µm, B – smoothing of the surface caused by friction and the accumulation of wear products in the friction area (red oval mark); friction in distilled water

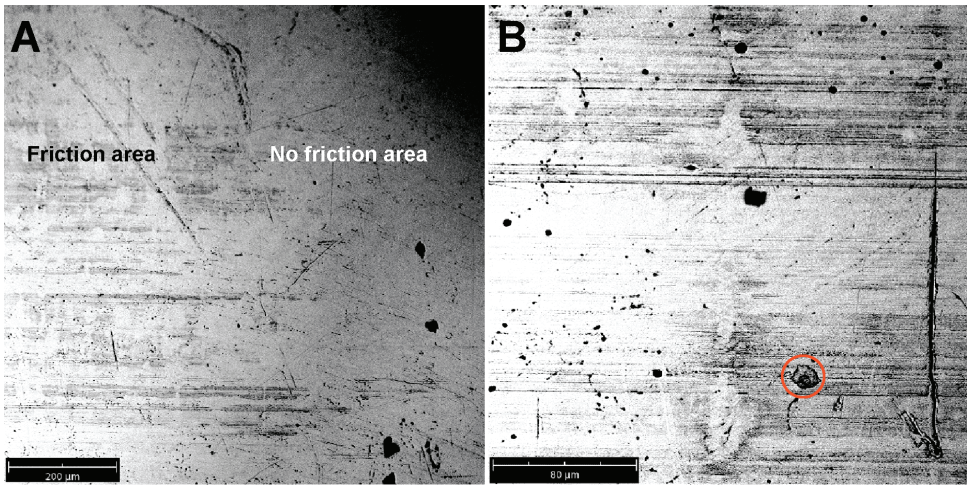

Fig. 14. Surface of the austenitic steel rod: A – border between the friction and non-friction area, B – wear on the surface of the rod caused by friction process; the red colour marks a loose particle that forms scratches and furrows on the surface of the rod; friction in the presence of acidic sodium lactate

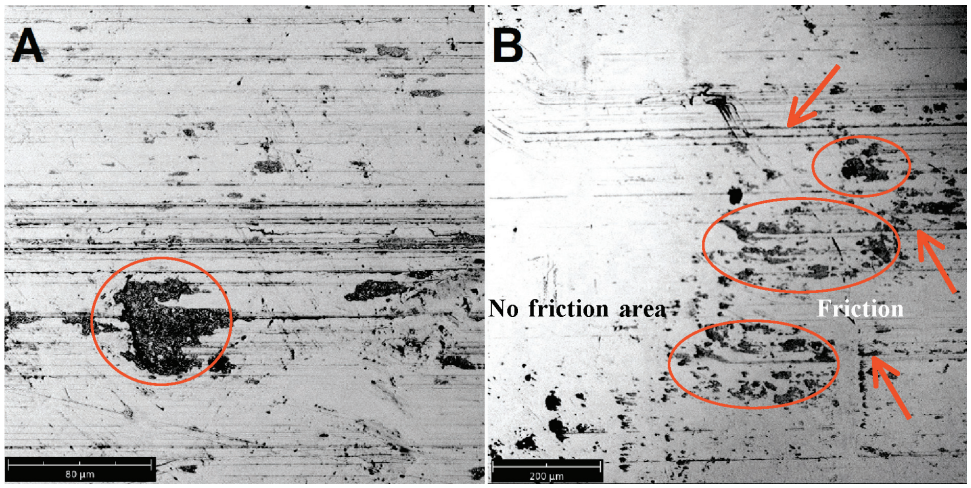

Fig. 15. Changes on the surface of the steel rod; A – wear products accumulated on the surface; the red colour marks a significant (~67 µm) wear product with an irregular, sharp-edged shape, B – borderline between the friction and non-friction area; in the friction area, numerous scratches and furrows (red arrows) and wear products (ovals) are visible; friction in distilled water

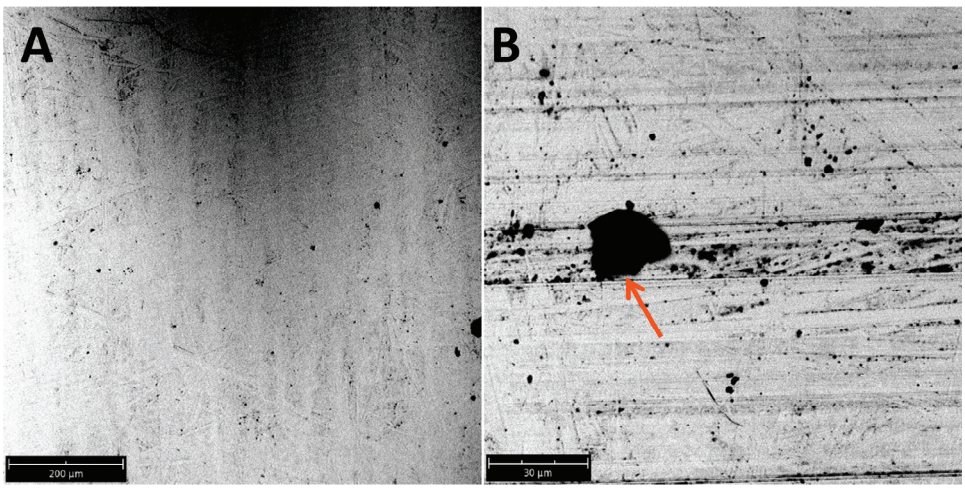

Fig. 16. Surface of the CoCrMo alloy rod: A – smooth surface before the friction process, B – visible traces of wear; loose, a hard particle causes a crack; friction in the presence of acid sodium lactate

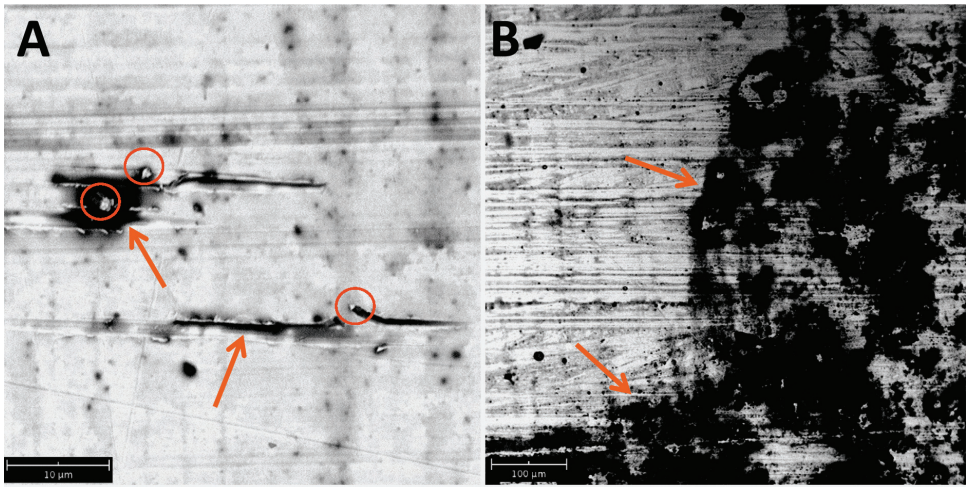

Fig. 17. Surface of the CoCrMo alloy rod: A – surface damage caused by loose particles (red ovals), arrows indicate visible furrowing effect, B – accumulation of wear products at the border of the friction and non-friction areas (dark areas in the picture); friction in an environment of acidic sodium lactate

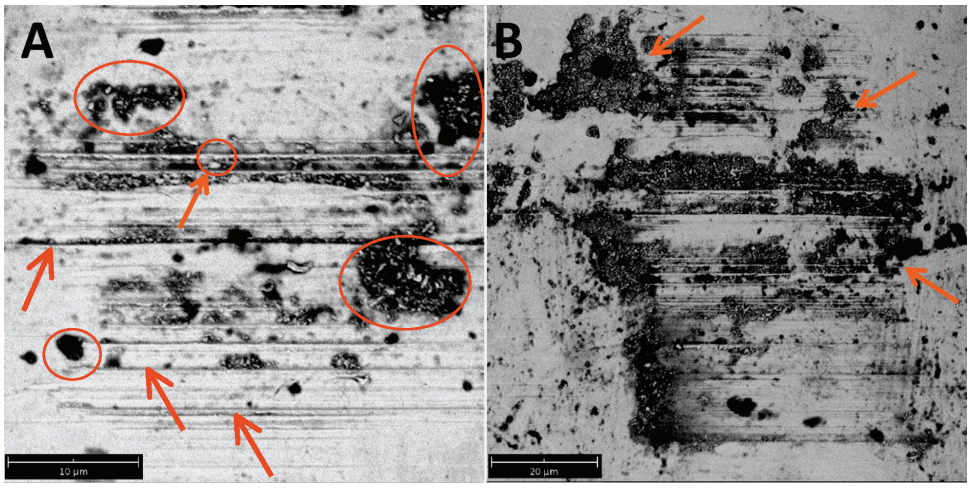

Fig. 18. Surface of the CoCrMo alloy rod: A – visible numerous furrows and scratches (arrows) caused by hard particles acting as an abrasive (oval marks), B – damage of the rod surface and accumulation of wear products at the border of the friction path; friction in distilled water

4. Discussion

4.1. Static friction measurement

When analysing the results of the static friction coefficient measurements, a clear impact of the number of completed traffic cycles on the static friction coefficient value is visible, which proves the important role of the friction process for these types of tribological joints. What is interesting is that the number of completed movement cycles has a different effect on the sliding pairs in which the rod is made of titanium alloys when compared to the effect on the pairs of the rods made of steel and cobalt-chrome alloy. For the rods made of both titanium alloys, i.e., Ti6Al4V and Ti6Al7Nb, the value of the static friction coefficient decreases with the number of completed movement cycles. This regularity is observed in both solutions and is indicated by the arrows in Fig. 7. For the rods made of 316L steel and CoCrMo alloy, which slide against each other in distilled water, the value of the static friction coefficient increases with the number of completed operating cycles. However, in the solution of acidic sodium lactate, no such tendency is observed for any of these materials.

It was also observed that after exceeding the wire tension force F_N = 150 N, the value of the static friction coefficient stabilizes in the case of the measurements carried out in the presence of acidic sodium lactate. Moreover, the static friction coefficient takes

on a decreasing tendency for the measurements carried out in distilled water.

The conducted measurements confirmed the impact of both the number of completed movement cycles and the value of the force loaded on the wire on the static friction coefficient.

4.2. Kinetic friction measurement

When analysing the effect of the number of completed movement cycles on the value of the kinetic friction coefficient (Fig. 8), it can be seen that similar values occur for the pairs with the Ti6Al4V and Ti6Al7Nb rods, as well as for the pairs with the steel and CoCr rod. For the sliding pairs with titanium alloys, much higher values of the kinetic friction coefficient were observed when compared to the pairs with the steel 316L and CoCrMo alloy, regardless of the applied lubricant. This is undoubtedly due to the much higher initial surface roughness value of the titanium rods than the austenitic steel rods. For all the tested material combinations, a slight stabilization of the kinetic friction coefficient value after about 10,000 movement cycles is observed, which may indicate that the running in process for the sliding pair is then finished.

The comparison of the kinetic friction coefficients for the distilled water and acidic sodium lactate demonstrates that the type of lubricant used affects the obtained measurement results in an uneven way. For the sliding pairs of the PE-UHMW wire with the titanium alloys Ti6Al4V and Ti6Al7Nb, the type of lubricant has a slight impact on the values of the kinetic friction coefficients. In addition, these values change slightly as the number of operating cycles increases. This means that they will exhibit high stability during operation. On the other hand, for the sliding pairs of the wire with the austenitic steel rod and CoCrMo alloy, a large impact of the lubricant on the values of the kinetic friction coefficients is observed. The results obtained for the distilled water are higher than those obtained for the acidic sodium lactate by 35–60% in the case of the combination with the austenitic steel, and 40–50% in the case of the combination with the CoCrMo alloy. This discrepancy increases with the number of operating cycles.

4.3. Analysis of the surface roughness of metal elements

When analysing the values of the *Sq* parameter presented in Table 3, the initial surface roughness of the austenitic steel was much lower than for the CoCrMo and titanium alloy rods. It can also be noted that the friction process had an uneven effect on the change of the surface roughness of the rods, depending on the rods material and the solution in which the friction joint was immersed. The biggest changes were observed for the steel rods in distilled water. The value of the surface roughness parameter *Sq* increased by 82%. On the other hand, surface roughness was reduced only by 7% after rubbing in acidic sodium lactate. For the rods made of CoCrMo, the friction process results in the decrease of surface roughness of about 34% in the case of ASL and 13% in the case of DW.

Concerning the titanium alloys, the friction process resulted in an increase of surface roughness parameters regardless of the lubricating solution. Rubbing in acidic sodium lactate influenced the significant increment of surface roughness about 49% for Ti6Al4V and 35% for Ti6Al7Nb. On the contrary, friction in distilled water, to a very small extent, increased the surface roughness – 5% for Ti6Al4V and 3% for Ti6Al7Nb.

It can be concluded that the greatest dispersion of surface roughness was observed in the distilled water environment.

4.4. Microscopic observations of the rod surface

The microscopic observations of the surface of the metal rods showed that the border between the non-friction area and the friction area is very blurred. The area where the friction could not be fully detected extends for about 1 to 3 millimetres (Fig. 12). This may be due to the uneven pressure distribution in the friction area, which may be associated with two factors. The first one is the construction of the braided polymer fibres and the associated high susceptibility of the tested wires. The second factor is the roughness of the surface layer of the metal rod, which may impede the close adhesion of the sliding surfaces (Figs. 10 and 12).

When polymer wires slide against the titanium alloy rods Ti6Al4V and Ti6Al7Nb, irregularities (most probably resulting from the passivation process) are smoothed, which effects in a reduction of its surface roughness (Figs. 10B and 12B).

During microscopic observations, numerous wear products are visible, including those that are compacted into conglomerates harder than the base material – probably metal oxides. These contribute to the

intensification of wear on the surface of the metal rods. The largest amounts of wear products were found near the border of the friction and non-friction areas. They were of different sizes depending on the material of the rod. In the case of the Ti6Al4V alloy, individual wear products ranging in size from 5 to 15 μm were observed and collected into conglomerates of about 30 μm in size (Fig. 11B). In turn, the largest single wear products observed on the surface of the Ti6Al7Nb rod reached the dimensions of 80 μm (Fig. 13A). The wear products from the steel rod were mostly about 15–20 μm in size, but there were also larger particles with an irregular, sharp-edged shape and a size of about 65 μm (Fig. 15A). In the case of the CoCrMo alloy rod, the smallest wear products were observed – from 1 to 5 μm (Fig. 17A and B) and less frequent larger particles with a size of about 10 μm (Fig. 18A). The scratches and furrows visible on the surface indicate the presence of all the mechanisms of abrasive wear in the overall wear process.

5. Conclusions

The problem of treating early-onset idiopathic scoliosis remains unresolved and represents a challenge for both doctors and engineers involved in designing growth-guiding implants. This was also the main reason for the interest in this subject and for undertaking research to broaden and supplement the knowledge of one of the stabilization systems offered on the market. The idea, based on an unconventional type of bearing, i.e., rod – polymer wire, is very interesting, innovative and has great potential for development.

The research carried out within the framework of this work extends the knowledge in this area. The impact of the number of movement cycles, in the range from 0 to 20 000, on changes in the values of the kinetic and static friction coefficients was analysed. Moreover, the impact of the load force on the friction node, in this case, the tensile force of polymer fibres in the range of 50–300 N, on the value of the static friction coefficient was shown. The measurements carried out at a stabilized temperature of 38 °C also show the impact of the type of lubricant on the values of friction coefficients.

From the observations made during the measurements, it can be concluded that the pairs with the austenitic steel and CoCrMo alloy showed the lowest values of friction coefficients, both static and kinetic, during the sliding cooperation of the metal rods with the PE-UHMW wires. The ease of sliding in these combinations proves that they are very promising with regards to movable stabilization systems that allow for spinal growth. This is undoubtedly due to the higher surface roughness value of Ti6Al4V and Ti6Al7Nb rods when compared to other materials.

Components made of polymer fibres, due to their specific construction, show interesting mechanical properties and tribological behaviour. The susceptibility of fibres and their derivatives makes tangential stresses inseparable from normal stresses, which is extremely interesting from the tribological point of view. This susceptibility also results in an increased resistance to wear of the polymer element. Unfortunately, the increase in resistance to wear of the polymer element can be combined with an increase in wear of the surface of the metal rod, and this should be the subject of further research.

On the other hand, thanks to the susceptibility of the fibres, it is possible to use the already known and proven sliding combination of polymer and metal as the simple fixing elements of rods for mobile scoliosis stabilization.

All these facts make the use of polymer fibres for the components of sliding bio-joints promising. At the same time, it should be stressed out that in the case of biomedical applications, the most important determinant of the usefulness of the fibres will be its wear, and this should therefore, be the subject of further comprehensive research.

References

[1] ADAMS M.A., HUTTON W.C., STOTT J.R., *The resistance to flexion of the lumbar intervertebral joint*, Spine (Phila. Pa. 1976), 1980, 5, 245–253.

[2] BĘDZIŃSKI R., *Engineering Biomechanics: selected issues*, Oficyna Wydawnicza Politechniki Wrocławskiej, 1997 (in Polish).

[3] BOGIE R., ARTS J.J., KOOLE S.N., VAN RHIJN L.W., WILLEMS P.C., *The Use of Metal Sublaminar Wires in Modern Growth-Guidance Scoliosis Surgery: A Report of 4 Cases and Literature Review*, Int. J. Spine Surg., 2020.

[4] BOGIE R., ROTH A., FABER S., WELTING T., WILLEMS P., ARTS J. et al., *Novel Radiopaque UHMWPE Sublaminar Wires in a Growth-Guidance System for the Treatment of Early Onset Scoliosis: Feasibility in a Large Animal Study*, Spine (Phila. Pa. 1976), 2014.

[5] BROŃCZYK A., KOWALEWSKI P., SAMORAJ M., *Tribocorrosion behaviour of Ti6Al4V and AISI 316L in simulated normal and inflammatory conditions*, Wear, 2019, 434–435, https://doi.org/10.1016/j.wear.2019.202966

[6] EL-SAYED A.A., EL-SHERBINY M.G., ABO-EL-EZZ A.S., AGGAG G.A., *Friction and wear properties of polymeric composite materials for bearing applications*, Wear, 1995, 184, 45–53.

[7] FEJDYŚ M., ŁANDWIJT M., *Technical fibers reinforcing composite materials* (in Polish), Tech. Wyr. Włókiennicze, 2010, 18, 12–22.

[8] FRIEDRICH K., LU Z., HAGER A.M., *Recent advances in polymer composites' tribology*, Wear, 1995, 190, 139–144.
[9] HUMMEL J.M., BOOMKAMP I.S.M., STEUTEN L.M.G., VERKERKE B.G.J., IJZERMAN M.J., *Predicting the health economic performance of new non-fusion surgery in adolescent idiopathic scoliosis*, J. Orthop. Res., 2012, 30, 1453–1458.
[10] IBRAHEM R.A., *Friction and wear behaviour of fibre/particles reinforced polyester composites*, Int. J. Adv. Mater. Res., 2016, 2, 22–26.
[11] JACOBS O., MENTZ N., POEPPEL A., SCHULTE K., *Sliding wear performance of HD-PE reinforced by continuous UHMWPE fibres*, Wear, 2000, 244, 20–28.
[12] KOWALEWSKI P., WIELEBA W., *Sliding polymers in the joint alloplastic*, Arch. Civ. Mech. Eng., 2007, 7, 107–119, https://doi.org/10.1016/S1644-9665(12)60229-5.
[13] KOWALEWSKI P., BROŃCZYK A., WIELEBA W., *A tribological test rig for fibres, cables, and plaitings*, Tribologia, 2017.
[14] KUJAWA M., KOWALEWSKI P., WIELEBA W., *The Influence of Deformation under Tension on Some Mechanical and Tribological Properties of High-Density Polyethylene*, Polymers, (Basel), 2019, 11, 1429.
[15] KUMAR P., OKA M., IKEUCHI K., SHIMIZU K., YAMAMURO T., OKUMURA H., KOTOURA Y., *Low wear rate of UHMWPE against zirconia ceramic (Y-PSZ) in comparison to alumina ceramic and SUS 316L alloy*, J. Biomed. Mater. Res., 1991, 25, 813–828.
[16] LI X.Y., DONG H., SHI W., *New insights into wear of Ti6Al4V by ultra-high molecular weight polyethylene under water lubricated conditions*, Wear, 2001, 250, 553–560.
[17] MEIJER G., *Development of a non-fusion scoliosis correction device. Numerical modelling of scoliosis correction*, 2011.
[18] PACH J., FRĄCZEK N., KACZMAR J., *The Effects of Hybridisation of Composites Consisting of Aramid, Carbon, and Hemp Fibres in a Quasi-Static Penetration Test*, Materials, (Basel), 2020, 13, 4686.
[19] RITUERTO SIN J., SUÑER S., NEVILLE A., EMAMI N., *Fretting corrosion of hafnium in simulated body fluids*, Tribol. Int., 2014, 75, 10–15, https://doi.org/10.1016/j.triboint.2014.03.003.
[20] RITUERTO SIN J., HU X., EMAMI N., *Tribology, corrosion and tribocorrosion of metal on metal implants*, Tribol. – Mater. Surfaces Interfaces, 2013, 7, 1–12, https://doi.org/10.1179/1751584X13Y.0000000022.
[21] ROHLMANN A., ZANDER T., BURRA N.K., BERGMANN G., *Flexible non-fusion scoliosis correction systems reduce intervertebral rotation less than rigid implants and allow growth of the spine: A finite element analysis of different features of orthobiom™*, Eur. Spine J., 2008, 17, 217–223, https://doi.org/10.1007/s00586-007-0480-1.
[22] ROTH A.K., BOGIE R., WILLEMS P.C., DE JONG J., VAN DEN BERGH J., ARTS J.J., *Novel Radiopaque Uhmwpe Sublaminar Wires in a Growth-guidance System for The Treatment of Early Onset Scoliosis: Feasibility in a Large Animal Model*, Spine J., 2002, 11, 137–144.
[23] ROTH A.K., BOON-CEELEN K., SMELT H., VAN RIETBERGEN B., WILLEMS P.C., VAN RHIJN L.W., ARTS J.J., *Radiopaque UHMWPE sublaminar cables for spinal deformity correction: Preclinical mechanical and radiopacifier leaching assessment*, J. Biomed. Mater. Res., Part B, Appl. Biomater., 2018, 106, 771–779.
[24] SAMORAJ M., *Tribocorrosion tests of materials applied for implants* (in Polish), Wrocław University of Science and Technology, 2014.
[25] SCHMALZRIED T.P., PETERS P.C., MAURER B.T., BRAGDON C.R., HARRIS W.H., *Long-duration metal-on-metal total hip arthroplasties with low wear of the articulating surfaces*, J. Arthroplasty, 1996, 11, 322–331.
[26] SHI W., DONG H., BELL T., *Tribological behaviour and microscopic wear mechanisms of UHMWPE sliding against thermal oxidation-treated Ti6Al4V*, Mater. Sci. Eng. A., 2000, 291, 27–36.
[27] STODOLAK E., *Research on surface modification and the influence of fibers on polymeric material and cellular response*, Doctoral Thesis, AGH, Kraków 2006 (in Polish).
[28] SURESHA B., CHANDRAMOHAN G., SAMAPTHKUMARAN P., SEETHARAMU S., VYNATHEYA S., *Friction and wear characteristics of carbon-epoxy and glass-epoxy woven roving fiber composites*, J. Reinf. Plast. Compos., 2006, 25, 771–782.
[29] WESOŁOWSKA M., DELCZYK-OLEJNICZAK B., *Fibers in ballistics – today and tomorrow* (in Polish), Tech. Wyr. Włókiennicze, 2011, 41–50.
[30] PubCHEM – National Library of Medicine. National Center for Biotechnology Information, (n.d.), https://pubchem.ncbi.nlm.nih.gov/compound/Sodium-lactate (Accessed: November 6, 2020).
[31] DailyMed – U.S. NATIONAL LIBRARY OF MEDICINE, (n.d.). https://dailymed.nlm.nih.gov/dailymed/archives/fdaDrugInfo.cfm?archiveid=2425 (Accessed: November 6, 2020).
[32] chemBlink – Online Database of Chemicals from Around the World, (n.d.). https://www.chemblink.com/products/72-17-3.htm (Accessed: November 6, 2020).